EuCARD-2

Enhanced European Coordination for Accelerator Research & Development

Journal Publication

Femtosecond timing-jitter between photo-cathode laser and ultra-short electron bunches by means of hybrid compression

Pompili, Riccardo (Laboratory Nazionali di Frascati) *et al*

12 August 2016

The EuCARD-2 Enhanced European Coordination for Accelerator Research & Development project is co-funded by the partners and the European Commission under Capacities 7th Framework Programme, Grant Agreement 312453.

This work is part of EuCARD-2 Work Package **13: Novel Acceleration Techniques (ANAC2)**.

The electronic version of this EuCARD-2 Publication is available via the EuCARD-2 web site <http://eucard2.web.cern.ch/> or on the CERN Document Server at the following URL: <http://cds.cern.ch/search?p=CERN-ACC-2017-0048>

Femtosecond timing-jitter between photo-cathode laser and ultra-short electron bunches by means of hybrid compression

2016 New J. Phys. 18 083033

(http://iopscience.iop.org/1367-2630/18/8/083033)

New Journal of Physics
The open access journal at the forefront of physics

Deutsche Physikalische Gesellschaft DPG
IOP Institute of Physics

Published in partnership with: Deutsche Physikalische Gesellschaft and the Institute of Physics

OPEN ACCESS

RECEIVED
21 March 2016

REVISED
17 June 2016

ACCEPTED FOR PUBLICATION
14 July 2016

PUBLISHED
12 August 2016

PAPER

Femtosecond timing-jitter between photo-cathode laser and ultra-short electron bunches by means of hybrid compression

R Pompili[1], M P Anania[1], M Bellaveglia[1], A Biagioni[1], G Castorina[1,2], E Chiadroni[1], A Cianchi[3], M Croia[1], D Di Giovenale[1], M Ferrario[1], F Filippi[4], A Gallo[1], G Gatti[1], F Giorgianni[4], A Giribono[4], W Li[5], S Lupi[4], A Mostacci[4], M Petrarca[4], L Piersanti[4], G Di Pirro[1], S Romeo[1], J Scifo[1], V Shpakov[1], C Vaccarezza[1] and F Villa[1]

[1] Laboratori Nazionali di Frascati, Via Enrico Fermi 40, I-00044 Frascati (Rome), Italy
[2] University of Catania, Piazza Universitá 2, I-95131 Catania, Italy
[3] University of Rome 'Tor Vergata', Via della Ricerca Scientifica 1, I-00133 Rome, Italy
[4] University Of Rome 'Sapienza', Piazzale Aldo Moro 5, I-00185 Rome, Italy
[5] National Synchrotron Radiation Laboratory, University of Science and Technology of China, Hefei, Anhui, 230029, People's Republic of China

E-mail: riccardo.pompili@lnf.infn.it

Keywords: beam dynamics, velocity-bunching, magnetic compression, synchronization, timing jitter, photo-injector

Abstract

The generation of ultra-short electron bunches with ultra-low timing-jitter relative to the photo-cathode (PC) laser has been experimentally proved for the first time at the SPARC_LAB test-facility (INFN-LNF, Frascati) exploiting a two-stage hybrid compression scheme. The first stage employs RF-based compression (velocity-bunching), which shortens the bunch and imprints an energy chirp on it. The second stage is performed in a non-isochronous dogleg line, where the compression is completed resulting in a final bunch duration below 90 fs (rms). At the same time, the beam arrival timing-jitter with respect to the PC laser has been measured to be lower than 20 fs (rms). The reported results have been validated with numerical simulations.

1. Introduction and motivation

The generation of ultra-short electron bunches is strongly driven by a wide range of applications spanning from high intensity radiation sources (e.g. free electron lasers [1] and THz [2]) to novel acceleration concepts (e.g. based on plasma wakefields [3]). Ultra-short bunches cannot be produced directly at low energies from the source due to space-charge forces acting within short distances [4] and scaling as γ^{-2}, being γ the relativistic Lorentz factor. For this reason and in order to preserve the beam brightness, a low peak current beam is usually generated and then compressed downstream the source [5].

In this paper we demonstrate and experimentally prove a hybrid compression scheme implemented at the SPARC_LAB test-facility [6] that simultaneously reduces the bunch duration and its arrival timing-jitter (ATJ) relative to the photo-cathode (PC) laser. A 50 pC electron beam is generated in the RF gun and then injected in the first accelerating section where it is accelerated and longitudinally over-compressed (head and tail reversed) by means of the velocity-bunching (VB) technique [7], acquiring a positive energy chirp. The beam is then sent in a non-isochronous dogleg line acting as a magnetic compressor [8]. The underlying principle of simultaneous bunch and jitter (with respect to the PC laser) compression relies on space-charge effects that, especially for ultra-short beams, strongly affect the longitudinal phase space (LPS), but are mostly ineffective on the bunch centroid dynamics (mean energy and time of arrival). It means that PC laser arrival time and RF accelerating field jitters have a different impact on the time-energy distribution of particles within the bunch (where space-charge must be considered) and on bunch centroids in consecutive shots (not affected by space-charge). By using this hybrid compression scheme we obtained a less than 90 fs (rms) bunch duration and an ATJ relative to the PC laser below 20 fs (rms) downstream the dogleg. It is worth pointing out that standard compression techniques exploit RF-induced energy chirps that lead to a reduction of the beam timing-jitter relative to the RF fields but at

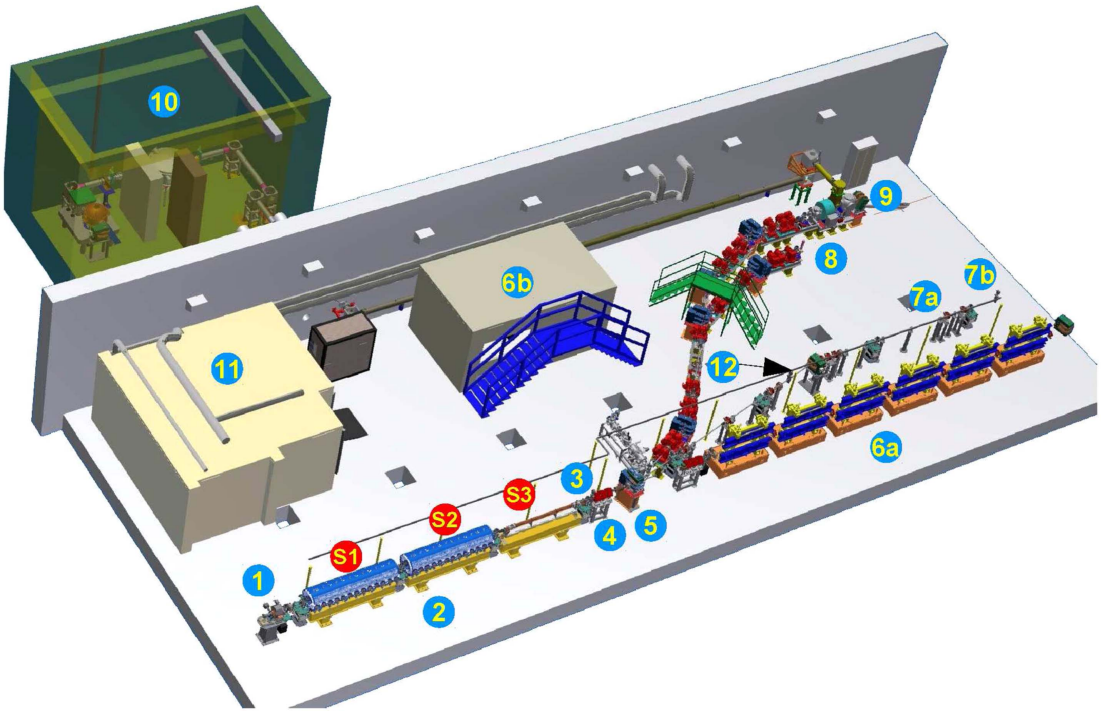

Figure 1. SPARC_LAB facility. The gun (1) is followed by the three accelerating sections (2), a THz source station (3) and a RF-Deflector (4). Four beamlines follows the dipole (5), devoted to FEL physics (6a) both in SASE and with seed-laser (6b), beam diagnostics based on THz radiation (7a) and EOS (7b), plasma acceleration (8) and x-rays production by Thomson scattering (9) using the FLAME laser (10). The EOS laser is split from the PC one (11), and delivered by an optical line (12).

the expense of the one relative to the PC laser. Previous works on this topic, obtained in several facilities, reported relative timing-jitters in the range of 50–100 fs [9–11].

The proposed method could be of great interest for applications like seeded-FEL [12] and x/γ-rays production by Thomson scattering [13] that need electron bunches to be precisely synchronized with a laser system. It represents also a key requirement for experiments foreseeing a fs-level synchronization like novel plasma accelerators employing the combined use of lasers and ultra-short bunches coming from a photo-injector [14, 15]. This scenario, in particular, is the most challenging since it requires relative timing-jitters well below 30 fs.

The paper is organized as follows. Section 2 reports the implementation of the hybrid scheme at SPARC_LAB. The theoretical background, together with a comprehensive description of the sources of time of arrival jitter, is reported in section 3. Section 4 describes the experiment setup, in particular the photo-injector working point and the dogleg magnetic lattice. A description of the diagnostics tools is presented as well. Finally, in section 5 we show the experimental results consisting in a final bunch duration of 86 fs (rms) with 19 fs (rms) timing-jitter relative to the PC laser. Measurements are validated by means of a comprehensive simulation study.

2. SPARC_LAB test-facility

SPARC_LAB [6] (LNF-INFN) is a test-facility providing electron bunches with energies up to 170 MeV feeding four experimental beamlines (figure 1). It is based on the combination of high brightness beams ($\approx 10^{15}$ A m^{-2} rad^{-2}) from the SPARC photo-injector [16] with high power laser pulses (300TW) from the FLAME facility [17]. The joint presence of these two systems allows the investigation of several plasma acceleration schemes, e.g. self [18] and external-injection [15], laser and beam-driven, and a wide spectrum of interdisciplinary leading-edge research activities based on novel radiation sources, such as free-electron laser (FEL) both in SASE, seeded and exotic schemes [1, 19], x-ray sources by means of Thomson scattering [20], high power THz radiation both broadband and narrow-band [21, 22].

2.1. Photo-injector

The SPARC photo-injector consists in a S-band 1.6 cell BNL/UCLA/SLAC type RF-gun providing 120 MV m^{-1} peak electric field on the built-in metallic (Cu) PC. Electrons are extracted by means of UV laser pulses ($\lambda = 266$ nm) whose shape and duration (0.1–10 ps FWHM) can be tailored to the needs of the

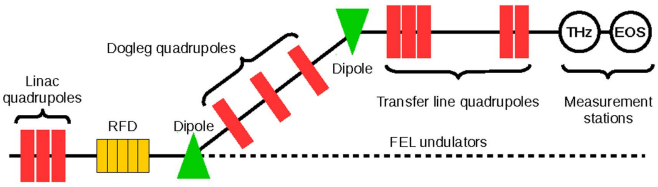

Figure 2. Dogleg layout and experimental devices used for longitudinal measurements.

aforementioned applications [23, 24]. They are accelerated up to 5.3 MeV in the gun [25] and then injected into three S-band sections (called S1, S2 and S3 in the following). S1 is also used as RF-compressor by means of VB [26, 27]. Solenoid coils embedding the first two sections can provide additional magnetic focusing during VB process and control of emittance and envelope oscillations [28]. A diagnostics transfer line, consisting in a spectrometer and a RF-deflector (RFD), allows a complete 6D beam characterization (LPS, projected and slice emittance [29, 30]).

2.2. Dogleg beamline

When the photo-injector is not operated in the FEL mode, the beam can be bent by a dipole magnet either by 14° towards the dogleg or by 25° towards the plasma acceleration and Thomson scattering beamlines. The dogleg is sketched in figure 2. It consists of three dispersion-matching quadrupoles placed between the two dipoles and five more focusing quadrupoles in the final straight path, that allow to match the dispersion-free beam through the beamline. Downstream the dogleg both the bunch length and the ATJ can be measured with an electro-optic sampling (EOS) system [31]. The bunch length measurement can be cross-checked through auto-correlation of coherent transition radiation (CTR) spectrum in THz range [32].

3. Theoretical background

The goal of this study is to combine VB and magnetic compression in a dogleg through a hybrid scheme providing short bunches ($\sigma_t < 100$ fs) with ultra-low timing-jitter relative to the PC laser system. For this purpose we proceed by fully characterizing the beam dynamics along the photo-injector and the dogleg line with numerical simulations (section 4) and experimental measurements (section 5). The dogleg shown in figure 2 employs three quadrupoles, installed in the dispersive region, in order to zero the horizontal dispersion D_x and its first derivative D_{px} (being p_x the horizontal momentum component) after the bent path. Instead, the longitudinal dispersion represented by the R_{56} term of the linear transport matrix $\mathbf{R}$, cannot be changed nor zeroed simply changing the quadrupole currents. For instance, it is $R_{56} \approx -5$ mm for a 100 MeV beam. Non-trivial methods are required to properly handle this term, such as an off-energy setup of the dogleg [33] or a beam trajectory variation within the quadrupoles [34]. In the latter case the expected contribution to the R_{56} is negligible, being of the order of tens of microns even assuming large (mm-scale) misalignment in the quadrupoles.

3.1. Longitudinal dynamics in a dogleg beamline

Being $\mathbf{X} = [x, x', y, y', z, \delta]$ the six-element vector representing the coordinates of a test particle (with x, y, z the positions, x', y' the divergences and δ the fractional longitudinal momentum deviation), the transformation of $\mathbf{X}$ produced by a system of magnetic elements can be represented as a power series expansion of the trace space coordinates. Therefore we can assume

$$(\mathbf{X}_f)_i = R_{ij}(\mathbf{X_0})_j + T_{ijk}(\mathbf{X_0})_j(\mathbf{X_0})_k + U_{ijkl}(\mathbf{X_0})_j(\mathbf{X_0})_k(\mathbf{X_0})_l + \cdots, \quad (1)$$

where $\mathbf{X_0}$ is the initial coordinate and R_{ij}, T_{ijk}, U_{ijkl} are the transport matrices of increasing order. The longitudinal coordinate z of the single particle evolves as

$$z_f \approx z_0 + R_{56}\delta_0 + T_{566}\delta_0^2, \quad (2)$$

where $\delta_0 = \sigma_E/E_0$ and $\sigma_E = E - E_0$ is the energy deviation of the particle from the reference energy E_0. In equation (2) higher order effects (mostly due to the U_{5666} term[6]) have been neglected. The energy deviation of the single particle depends on its longitudinal position with respect to the RF wave during the acceleration process. Therefore δ_0 is a function of z

[6] For the dogleg beamline it results $U_{5666} \approx 2T_{566}$, i.e. $U_{5666} = \mathcal{O}(T_{566})$. Being $\delta_0 \ll 1$, it follows that $U_{5666}\delta_0^3 \ll T_{566}\delta_0^2$.

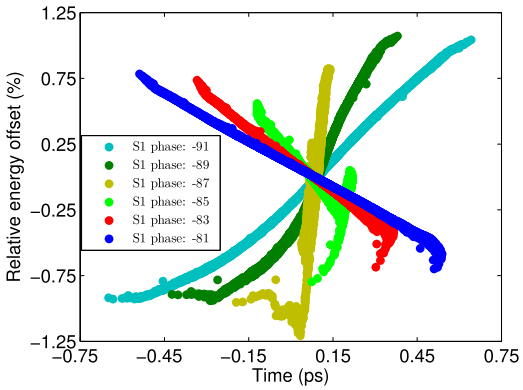

Figure 3. LPS of a 50 pC beam at the exit of the linac for different S1 injection phases. Early (late) particles correspond to greater (smaller) time values on the horizontal axis.

$$\delta_0(z_0) = \delta_u + h_1 z_0 + h_2 z_0^2 + \cdots, \tag{3}$$

where δ_u denotes the uncorrelated energy offset and h_1 and h_2 are the first and second order *chirp* terms, respectively. Dropping the single particle assumption, equations (2) and (3) can be combined to quantify the expected bunch length $\sigma_{z,f}$ at the end of a dispersive beamline [35]

$$\sigma_{z,f}^2 = R_{56}^2\sigma_{\delta_u}^2 + (1 + h_1 R_{56})^2\sigma_{z,i}^2 + 3(h_2 R_{56} + T_{566}h_1^2)^2\sigma_{z,i}^4, \tag{4}$$

where σ_{δ_u} is the uncorrelated (normalized) energy spread and $\sigma_{z,i}$ is the initial bunch length. According to equation (4), the minimum of $\sigma_{z,f}$ can be found by canceling the last two terms. This leads to

$$h_1 = -\frac{1}{R_{56}}, \tag{5}$$

$$h_2 = -\frac{T_{566}}{R_{56}}h_1^2 = -\frac{T_{566}}{R_{56}^3} \tag{6}$$

and the compression results more efficient at high energies ($\sigma_{\delta_u} \to 0$).

The previous formulation has to be modified if the beam energy $\widetilde{E}$ has an offset $\Delta = (\widetilde{E} - E_0)/E_0$ with respect to the reference energy E_0 [33]. In this case, a particle with arbitrary energy E has an energy error $\tilde{\delta} = (E - \widetilde{E})/\widetilde{E}$ relative to the *central* energy of the beam, and an energy error δ relative to the *design* energy of the beamline. By applying the coordinate transformation $\delta \to (\widetilde{E}/E_0)\tilde{\delta} + \Delta$, equation (2) modifies as

$$z_f \approx z_0 + \widetilde{Q_5} + \widetilde{R}_{56}\tilde{\delta} + \widetilde{T}_{566}\tilde{\delta}^2, \tag{7}$$

where $\widetilde{Q_5} = R_{56}\Delta + T_{566}\Delta^2$ and the linear and nonlinear transport terms are rewritten as follows:

$$\widetilde{R}_{56} = \frac{\widetilde{E}}{E_0}(R_{56} + 2T_{566}\Delta), \tag{8}$$

$$\widetilde{T}_{566} = \left(\frac{\widetilde{E}}{E_0}\right)^2 T_{566}. \tag{9}$$

Equation (7) represents the *effective* longitudinal transformation. Therefore, equation (4) has to be modified by replacing the R_{56} and T_{566} terms with the ones in equations (8) and (9).

3.2. Velocity-bunching technique

Following equation (5), the bunch compression in a dogleg with $R_{56} < 0$ is obtained if the chirp is positive (particles with higher energies on the head) and equal to $h_1 \approx \frac{1}{\sigma_z}\frac{\sigma_E}{E_0} = -\frac{1}{R_{56}}$. This can be fulfilled with a proper choice of energy (E_0), energy spread (σ_E) and length (σ_z). Short beams with positive chirp can be obtained with the VB scheme, using S1 as a RF compressor.

Starting from the cathode, the bunch is accelerated in the RF-gun where space-charge forces gradually lead to its lengthening, depending on the initial transverse and longitudinal profiles [36]. Figure 3 reports the simulated LPS of a 50 pC beam for several injection phases in S1. Early (late) particles correspond greater (smaller) time values on the horizontal axis. The simulation is performed with general particle tracer (GPT) [37], a PIC code that accounts for space-charge effects. On the cathode we used a laser pulse with longitudinal ($\sigma_t = 450$ fs) and transverse ($\sigma_{x,y} = 150\ \mu$m) gaussian profiles. The beam is then accelerated, resulting in a duration $\sigma_t \approx 830$ fs ($\sigma_z \approx 250\ \mu$m) at the gun exit. In VB the beam is injected in S1 forward-off-crest, i.e.

towards negative RF phases. The process is based on a correlated time-velocity chirp in the electron bunch, in such a way that electrons on the tail of the bunch are faster than electrons in the bunch head. This leads to a rotation of the LPS if the injected beam is slower than the phase velocity of the RF wave. So when it is injected at the zero-crossing field phase, it slips back to phases where the field is accelerating, but it is simultaneously chirped and compressed. As showed in figure 3, by moving towards negative phases the chirp is negative up to the maximum compression ($\phi_{S1} = -88^\circ$ with respect to the maximum energy phase), corresponding to a bunch duration $\sigma_t \approx 50$ fs ($\sigma_z \approx 15$ μm). Then, at even more negative phases (over-compression), it slightly elongates while the chirp becomes positive.

3.3. Time of arrival jitter sources

Longitudinal beam dynamics is sensitive to RF field fluctuations in the gun and accelerating sections. Fluctuations in the magnetic field of dispersive elements located along the machine can contribute too [38]. The energy, energy spread and duration of the beam are consequently affected, depending on the photo-injector configuration. The beam time of arrival is also influenced, resulting in an ATJ at the end of the line. We can define the ATJ as the shot-to-shot time of arrival fluctuation of the beam center of mass with respect to a fixed position. The ATJ is produced by several sources, e.g. the changing of the laser arrival time on the PC (Δt_{laser}), or instabilities in the timing (Δt_{RF}) of the RF system. In our discussion we do not consider fluctuations in the amplitude of RF and magnetic fields. If compared to the other jitter sources described in the following, their contribution to the overall ATJ is negligible[7].

At SPARC_LAB, the synchronization system operates by distributing a RF signal generated in a μ-wave reference master oscillator (RMO) through a coaxial cable star network. The client lock-in is then performed with electronic PLLs, resulting in less than 50 fs (rms) timing-jitter between the RMO and the PC laser system [39]. Downstream the photo-injector, the ATJ arises from three main sources: the PC laser and the two S-band klystrons; the first (K1) feeds the gun, S3 and the RFD while the other (K2) powers S1 and S2. For a given configuration, the beam arrival time variation Δt_{linac} can be expressed as a linear combination

$$\Delta t_{\text{linac}} \approx \sum_{i=1}^{3} c_i \Delta t_i, \tag{10}$$

where $i = 1, 2, 3$ refer, respectively, to the PC laser, K1 and K2 terms If the dogleg is included, equation (10) becomes

$$\Delta t_{\text{dogleg}} \approx \sum_{i=1}^{3} (c_i + h_{1,i} R_{56}) \Delta t_i. \tag{11}$$

The $h_{1,i}$ terms are related to energy fluctuations

$$\frac{\Delta E_0}{E_0} \approx c \sum_{i=1}^{3} h_{1,i} \Delta t_i, \tag{12}$$

where c is the speed of light and E_0 is the bunch energy. If the laser and RF fields are delayed all together by a given value, the beam arrival time is delayed by the same amount while the final energy remains unchanged. Therefore the following conditions apply:

$$\sum_{i=1}^{3} c_i = 1 \qquad \text{and} \qquad \sum_{i=1}^{3} h_{1,i} = 0. \tag{13}$$

All Δt_i values are measured with respect to the RMO. Since they are mostly uncorrelated, we can write the standard deviations values of equations (10) and (11) as

$$\sigma^2_{t_{\text{linac}}} \approx \sum_{i=1}^{3} c_i^2 \sigma^2_{t_i}, \tag{14}$$

$$\sigma^2_{t_{\text{dogleg}}} \approx \sum_{i=1}^{3} (c_i + h_{1,i} R_{56})^2 \sigma^2_{t_i}. \tag{15}$$

They represent the expected absolute ATJ (with respect to the RMO) at the linac and dogleg exit respectively. Their evaluation is provided in section 4.

[7] The RF and magnetic field jitters are, respectively $\Delta V_{\text{RF}}/V_{\text{RF}} < 0.08\%$ and $\Delta B/B \approx 0.01\%$. From these values the expected timing-jitters are less than 10 fs and 3 fs, respectively.

Table 1. Beam parameters in the VB configuration. The values reported between brackets refer to simulated data.

Laser parameters	**Value (sim.)**	**Unit**
X(Y) spot (rms)	230 ± 5 (230)	μm
Pulse duration (rms)	450 ± 50 (450)	fs
Beam parameters	**Value (sim.)**	**Unit**
Charge	50 ± 2 (50)	pC
Energy	81.2 ± 0.1 (81)	MeV
Energy spread (rms)	400 ± 10 (410)	keV
Duration	68 ± 18 (65)	fs
Norm. emittance (rms)	1.7 ± 0.2 (1.8)	μm

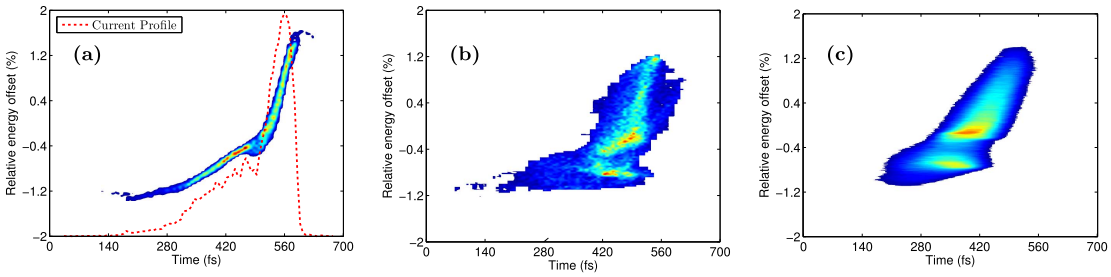

Figure 4. (a) Simulated LPS at the end of the linac The current profile is represented by the red dashed line. (b) Simulated LPS considering the quadrupoles, RFD and spectrometer between the linac exit and the screen where LPS is actually measured. (c) Experimentally measured beam LPS.

4. Setup of the experiment

In this section the SPARC_LAB photo-injector working point and the dogleg magnetic setup are described. At linac exit, a S-band RFD [40] is used to measure the bunch length. On the dogleg side, the beam longitudinal profile is obtained by means of a Michelson interferometer [41] measuring CTR and an EOS system [31]. These devices are described in section 5. The photo-injector working point is discussed in section 4.1 by means of a GPT start-to-end simulation (including space-charge effects) and a direct comparison with measurements is reported. An estimation of the beam ATJ at linac exit is then provided in section 4.2. Section 4.3 describes the relative ATJ reduction principle by exploiting the off-energy setup of the dogleg beamline. Then, in section 4.4, the dogleg setup is illustrated and validated by means of GPT simulations.

4.1. Setup of the photo-injector

The PC laser is configured as reported in table 1. Setting the linac for maximum energy gain (*on crest* configuration), the bunch has 164 MeV energy (90 keV energy spread), 1 ps (rms) duration and 1.1 μm (rms) normalized emittance. The beam is then longitudinally compressed with VB and its LPS is manipulated in order to match the dogleg (see 3.1). The final energy (81.2 MeV) and energy spread (0.4 MeV) are obtained by tuning the S2 and S3 phases. With 81.2 MeV energy, the dogleg transport matrix terms result $R_{56} = -4.5$ mm and $T_{566} = -83.6$ cm. According to equation (5), such R_{56} value requires an $h_1 = -R_{56}^{-1} \approx 222$ m^{-1} chirp at the dogleg entrance. In order to avoid an excessive emittance growth, the S1 embedded solenoids are turned on, in order to adopt the emittance compensation scheme [28]. The achieved emittance is 1.7 μm (rms). The resulting bunch (68 fs, rms) with positive chirp is obtained by moving the S1 injection phase by $-88°$ with respect to its *on crest* value, i.e. 1° beyond the maximum compression (50 fs, rms). All relevant parameters are reported in table 1.

Figure 4(a) shows the simulated time-energy distribution. Experimentally the LPS is retrieved by measuring the bunch time and energy profiles with the RFD and a magnetic spectrometer, respectively. By means of three quadrupoles, the resulting beam is then imaged on a screen located 3 m downstream the spectrometer. The effects of the quadrupoles and the RFD on the simulated beam LPS have been considered in figure 4(b). Its overall shape and inner structure are in good agreement with the measured LPS in figure 4(c). By performing a 2nd order polynomial fit to the simulated data in figure 4(a), we found $h_1 = 204.1$ m^{-1}, $h_2 = 1.5 \times 10^7$ m^{-2} and 60 keV uncorrelated energy spread (see equation (3)). According to equation (4), with such values the

Table 2. ATJ coefficients (equation (15)) from measurements and simulations (reported in brackets). The S1 injection phase in VB is set at -88° with respect to the *on crest* one.

Parameter	On crest	VB
c_1	$0.7 \pm 0.2\,(0.66)$	$-0.1 \pm 0.4\,(-0.14)$
c_2	$0.3 \pm 0.1\,(0.34)$	$-0.2 \pm 0.5\,(-0.07)$
c_3	$0.1 \pm 0.9\,(0.01)$	$1.2 \pm 0.5\,(1.18)$
$h_{1,1}$ (m^{-1})	$-1.8 \pm 1.2\,(-0.8)$	$-93 \pm 22\,(-90)$
$h_{1,2}$ (m^{-1})	$-0.6 \pm 1.2\,(-0.4)$	$41 \pm 23\,(38)$
$h_{1,3}$ (m^{-1})	$2.8 \pm 2.5\,(1.2)$	$42 \pm 35\,(52)$

expected bunch duration downstream the dogleg is $\sigma_t \approx 77$ fs, indicating that the nonlinear T_{566} and h_2 terms introduce non-negligible effects.

4.2. Measurement of the ATJ at linac exit

As previously mentioned, the bunch timing-jitter can be measured either with the RFD or the EOS [9]. In the first case the jitter is relative to the RF reference while in the second one the is relative to the EOS laser system. As pointed out in section 3.3, the total ATJ can be expressed as a linear combination of several jitter sources. For the evaluation of the c_i and $h_{1,i}$ coefficients, a GPT simulation has been performed. Here the PC laser time of arrival is, in turn, delayed or anticipated with respect to the linac RF accelerating phase. Finally, the beam time of arrival and its central energy are recorded on a fixed screen located at the exit of the linac Results are reported in table 2.

The simulated coefficients have been cross-checked with experimental measurements obtained by acquiring ten consecutive images on the first Ce:YAG screen located after the main dipole, with RFD turned on. In this case each image contains both the temporal and energy information. The c_1 (h_1) coefficient is obtained by measuring the beam time of arrival (energy) while varying the PC laser timing on the cathode. Similarly, the $c_{2,3}$ ($h_{2,3}$) coefficients are evaluated, respectively, by changing the RF field phase (i.e. its timing) on the K1 (gun) and K2 (S1) lines. Such coefficients allow to estimate all the jitter sources contained in equation (14). Table 2 highlights two main aspects. First, in the *on crest* case, the PC laser timing-jitter is compressed by a factor $c_1 = 0.66$ in the gun [42], meaning that beam dynamics is mostly determined by the PC laser ($c_1 > c_2 > c_3$). Second, in VB the longitudinal compression strongly links the beam to the S1 fields ($c_3 \gg c_{1,2}$) but a correlation between the PC laser and the beam energy still holds ($h_{1,1} = -90$). As explained in section 3.3, the SPARC_LAB power system employs two klystrons. If we measure the beam ATJ (downstream the linac) relative to the the RF system (K1 line) with the RFD, equation (14) becomes

$$\sigma^2_{t_{\mathrm{linac}}} \approx c_1^2\sigma^2_{t_{\mathrm{L}}} + (c_2 - 1)^2\sigma^2_{t_{\mathrm{K1}}} + c_3^2\sigma^2_{t_{\mathrm{K2}}}. \tag{16}$$

From equation (16), we can discriminate the contributions of the various jitter sources. For instance, if the linac is operated in the *on crest* configuration, the PC laser is the leading jitter source ($\sigma_{t_{\mathrm{L}}}$). Therefore the beam time of arrival mainly follows the PC laser timing. On the contrary, in VB regime the beam timing is strongly linked to the RF fields in S1, and its ATJ measured with RFD is actually due to $\sigma_{t_{\mathrm{K2}}}$. In this case the PC laser timing has a negligible effect.

Figure 5 reports the beam time of arrival in the *on crest* and VB configurations for 40 consecutive shots measured with the RFD by streaking the beam on a Ce:YAG screen. The emitted light is then imaged on a CCD, where each pixel corresponds to 18 fs. The resulting rms is $\sigma_{t_{\mathrm{linac}}} \approx 34$ fs in both cases. According to equation (16) and table 2, this corresponds to a PC laser jitter of $\sigma_{t_{\mathrm{L}}} \approx 48$ fs and an RF system jitter of $\sigma_{t_{\mathrm{K1}}} \approx \sigma_{t_{\mathrm{K2}}} \approx 22$ fs, compatible with previous measurements [39]. Assuming the PC laser as the reference, equation (16) becomes

$$\sigma^2_{t_{\mathrm{linac}}} \approx (c_1 - 1)^2\sigma^2_{t_{\mathrm{L}}} + c_2^2\sigma^2_{t_{\mathrm{K1}}} + c_3^2\sigma^2_{t_{\mathrm{K2}}}, \tag{17}$$

corresponding to a relative ATJ of $\sigma_{t_{\mathrm{linac}}} \approx 60$ fs between the electron beam and the PC laser at linac exit.

4.3. Relative ATJ reduction with the hybrid scheme

When a bunch is compressed in a non-isochronous magnetic line, its timing-jitter relative to the RF system (that has the initial energy chirp imprinted on it) is compressed too. On the contrary, the timing-jitter relative to the PC laser increases, since the beam results more linked to the RF system and uncorrelated from the laser time of arrival on the cathode. According to equation (15) we demonstrate that, with a proper correlation between shot-to-shot time of arrival and beam central energy, the hybrid scheme is able to manage simultaneously the bunch-to-laser jitter reduction and its longitudinal compression. Downstream the dogleg line, measurements have been performed by the EOS system. Since its probe laser is directly split from the PC laser, the ATJ relative to the

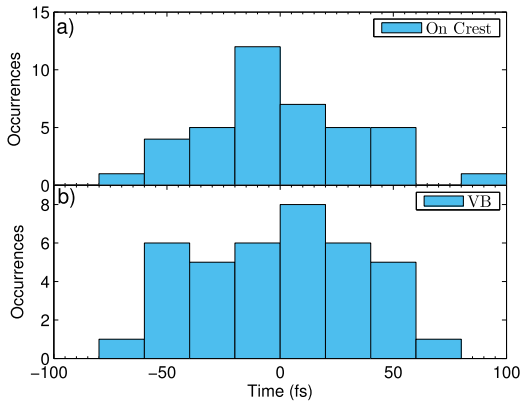

Figure 5. Beam time of arrival in the *on crest* (a) and VB (b) configurations measured with RFD. The rms of the distributions is approximately 34 fs in both cases.

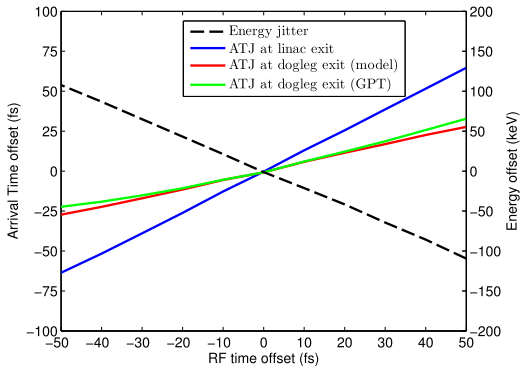

Figure 6. Beam arrival time-(blue) and energy-offset (black-dashed) at linac exit as a function of the RF time-offset. The ATJ (relative to the PC laser) at dogleg exit is calculated with the linear model (red) and simulated by GPT (green).

PC laser is given by

$$\sigma^2_{t_{\text{dogleg}}} \approx (c_1 + h_{1,1}R_{56} - 1)^2\sigma^2_{t_{\text{L}}} + (c_2 + h_{1,2}R_{56})^2\sigma^2_{t_{\text{K1}}} + (c_3 + h_{1,3}R_{56})^2\sigma^2_{t_{\text{K2}}}. \tag{18}$$

For the relative ATJ reduction, we exploited the off-energy beam transport through the dogleg (see section 3.1) in order to manipulate the R_{56}. By setting the design energy 0.18 MeV below the 81.2 MeV nominal beam energy ($\Delta = 2.2 \times 10^{-3}$), it results $\widetilde{R}_{56} = -8.2$ mm and $\widetilde{T}_{566} = -83.9$ cm with a $\sigma_{\text{t}} \approx 90$ fs (rms) expected bunch duration at the dogleg exit (see equation (4)). According to equation (18) we foresee a relative ATJ of $\sigma_{t_{\text{dogleg}}} \approx 26$ fs, about two times lower than $\sigma_{t_{\text{linac}}} \approx 60$ fs obtained in section 4.2.

Results are reported in figure 6 as a function of the RF field timing-jitter. There is a correlation between the shot-to-shot time of arrival (blue line) and energy (black-dashed line) of the over-compressed beam downstream the linac This means that bunches arriving earlier (later) have higher (lower) energies and they are delayed (anticipated) by the dogleg. The time reference is assumed to be the PC laser, thus a lower slope of the solid lines corresponds to a lower relative jitter. The ATJ reduction from $\sigma_{t_{\text{linac}}} \approx 60$ fs down to $\sigma_{t_{\text{dogleg}}} \approx 25$ fs is confirmed by the model of equation (11) (red line) and the GPT simulations[8] (green line).

The underlying principle for the simultaneous bunch compression and relative ATJ reduction relies on the differences in dynamics between particles in the same bunch and bunches in different shots. By means of the hybrid scheme we used VB in order to shorten the duration of the low energy (5.3 MeV) beam exiting from the gun. In these conditions space-charge forces strongly affect the beam LPS. On the contrary, the time-of-flight and mean energy are not perturbed. To clarify this principle we assumed each bunch centroid as a single particle so that the centroid distribution over consecutive shots can be considered as a unique space-charge-free beam, as showed by red dots in figure 7. The simulated single-shot bunch LPS evolution, including space-charge effects, is highlighted by blue dots. Figure 7(a) shows the beam LPS at the gun exit. As discussed in section 4.2, in this case the time of arrival is mainly linked to the release time from the cathode as reported in figure 7(d). The resulting

[8] The difference (few fs) between the model and GPT simulation is due to the T_{566} term, not considered in the (linear) model.

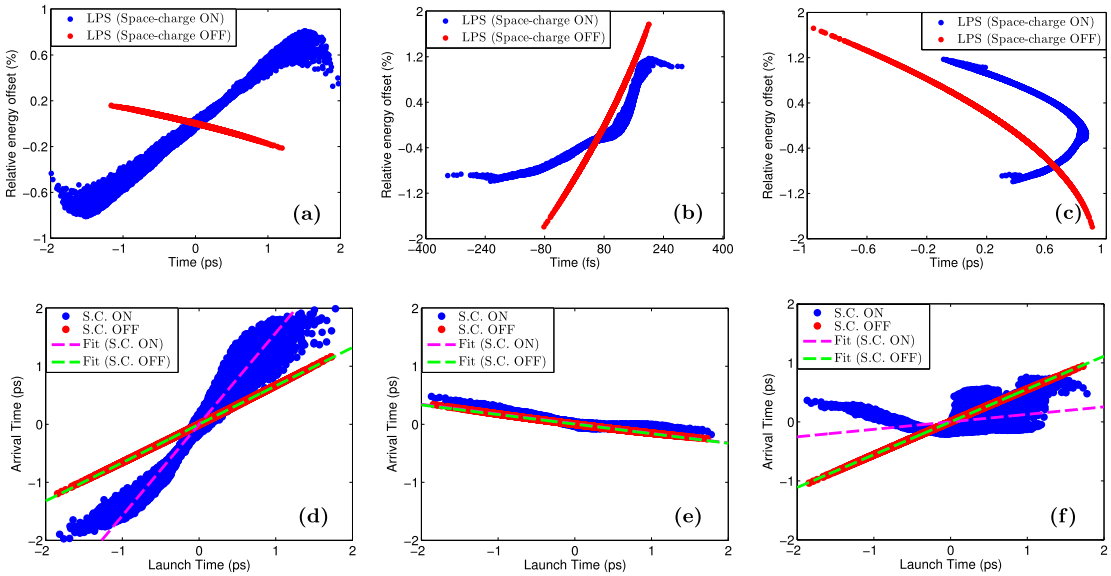

Figure 7. (a)–(c) Beam LPS (blue dots) and corresponding space-charge free distribution (red dots) simulated, respectively, at the exit of the gun (a), linac (b) and dogleg (c). (d)–(f) Time of emission from the cathode versus the time of arrival at the exit of gun (d), linac (e) and dogleg (f). The degree of correlation is represented by the linear fits (dashed lines).

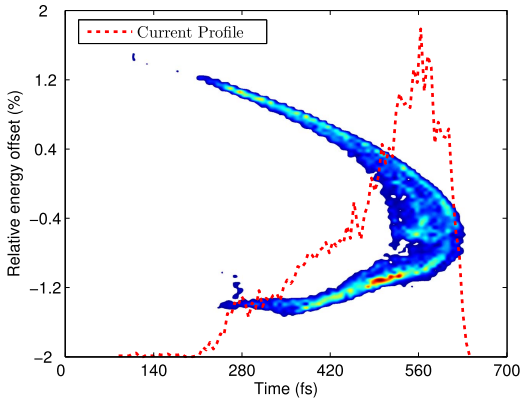

Figure 8. Simulated LPS at the end of the dogleg. The current profile is represented by the red dashed line.

correlation term is $c_1 = 1.58$ ($c_1 = 0.66$, see table 2). Downstream the gun, the beam is longitudinally compressed by VB and strongly linked to the RF field phase-jitter (figure 7(b)). Consequently, at the linac exit its time of arrival showed in figure 7(e) is not linked to the PC laser ($c_1 \approx -0.14$, see table 2). At this point, the correlation between the PC laser and the time-of-flight is restored by the dogleg. The different dynamics between the bunch inner structure and its longitudinal centroid allows us to reduce the ATJ relative to the PC laser in the dogleg while preserving its duration (figure 7(c)). Figure 7(f) shows that bunch length is compressed ($c_1 = 0.12$) while the correlation between the centroids (red dots) and the PC laser is partly recovered ($c_1 = 0.56$). This result represents a compromise between relative ATJ reduction and maximum achievable bunch compression.

4.4. Setup of the dogleg line

As explained in section 4.3, the off-energy setup of the dogleg allows to handle the R_{56} term in order to achieve the relative timing-jitter reduction. The dogleg matching is obtained with the MAD-X code [43], by constraining to zero the dispersion and its first derivative downstream the second dogleg dipole. The matching parameters are then imported in GPT in order to perform a full simulation including space-charge. From the resulting LPS, shown in figure 8, we evaluated a final bunch duration of 92 fs (rms), in agreement with the one expected according to equation (4) (90 fs, rms). If we consider that in the *on-crest* configuration the bunch duration was 1 ps (rms), the corresponding compression factor using the hybrid scheme is $C \approx 11$.

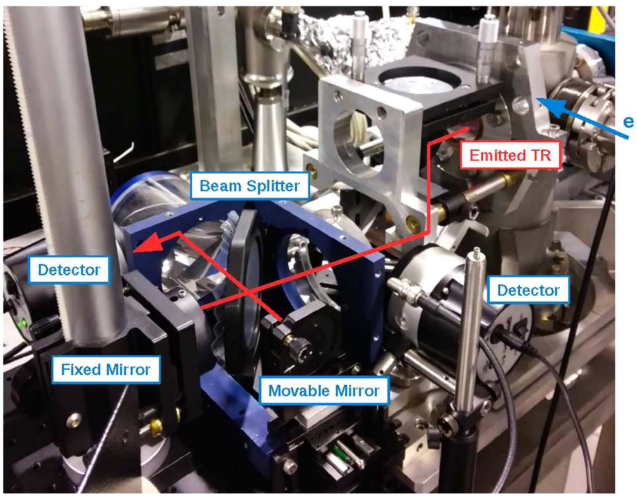

Figure 9. Michelson interferometer used in the experiment. The setup implements two detectors measuring the auto-correlated signal and a constant signal, acting as reference.

5. Experimental results

This section reports the results obtained with Michelson interferometer and EOS systems. These devices are able to measure the beam longitudinal profile in a multi-shot and single-shot way, respectively. The Michelson interferometer, in particular, is able to achieve a temporal resolution of $\sigma_t \approx 20$ fs on the bunch duration, while the EOS is used in order to monitor the beam ATJ with respect to the PC laser.

5.1. Michelson interferometer

The Michelson interferometer, schematically shown in figure 9, consists of two highly polished mirrors and a 12 μm mylar layer acting as a beam-splitter for the incoming CTR. In our setup CTR is produced by electron bunches crossing an aluminum-coated silicon screen oriented at 45° with respect to the beam line. Only the backward transition radiation is collected. It is extracted through a diamond window and collimated by a 90° off-axis parabolic mirror towards a flat mirror reflecting the radiation to the interferometer. The light is then split in two beams. One is transmitted towards a fixed mirror while the other is reflected in the direction of a movable one. The beams are then recombined on the beam-splitter and are measured by a pyro-electric detector provided by Gentec^{TM} (0.5–30 THz spectral range, 140 kV W^{-1} sensitivity). The radiation is collected by the detector at several positions of the movable mirror, producing an interference pattern used to reconstruct the beam temporal profile with a resolution $\sigma_t \approx 20$ fs (rms) [44].

5.1.1. Bunch duration measurements

Data have been acquired by changing the position of the interferometer movable mirror with 10 μm steps. At each position, five references and auto-correlation signals are acquired by two pyro-electric detectors and then averaged in order to take into account fluctuations in the beam charge (of the order of 5%). Each point is then used to make the interferogram of figure 10, from which the bunch frequency spectrum is retrieved. In order to reconstruct the bunch temporal profile from the interferogram, the effect of the finite-size of the CTR screen has been considered [45]. It introduces a suppression of the radiated intensity at low-frequencies (i.e. long wavelengths λ) when the extent of the particle field, which is of the order of $\gamma\lambda$, exceeds the dimension of the screen (30 $\times$ 30 mm). This is always the case for coherent radiation at THz frequency, and in our case it leads to a suppression of frequency components below 0.5 THz. To compensate these losses in the CTR spectrum, we introduced a low frequency Gaussian reconstruction. The electron bunch profile $S(z)$ is then retrieved from the form factor, applying Kramers–Kronig relations [46]. The reconstructed bunch profile is shown in the inset of figure 10. The retrieved duration is $\sigma_t = 86 \pm 7$ fs (rms), in good agreement with expectations of section 4.4. The result confirms that the bunch slightly elongated due to the larger R_{56} term resulting from the dogleg off-energy setup.

5.2. Electro-optic sampling

The EOS is a non-intercepting and single-shot device that allows to monitor the bunch longitudinal profile and time of arrival [47]. At SPARC_LAB we employ a 100 μm-thick gallium phosphide (GaP) crystal and a Ti:Sa

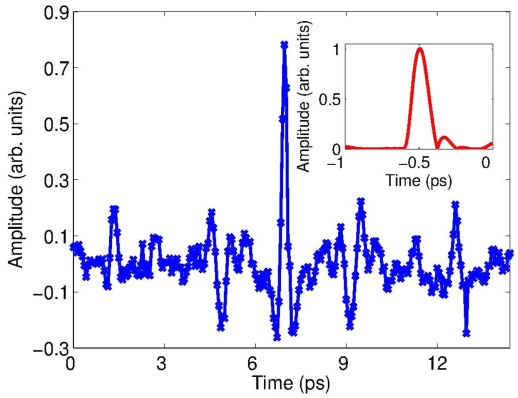

Figure 10. Interferogram obtained with Michelson interferometer. The inset shows the retrieved bunch temporal profile. The resulting in bunch duration is $\sigma_t = 86 \pm 7$ fs (rms).

laser ($\lambda = 800$ nm, 80 fs rms) as probe, fixing the EOS resolution on the bunch duration to $\sigma_t \approx 90$ fs (rms). The EOS input layout is shown in figure 11(a). The probe laser is split directly from the PC laser oscillator and then amplified, resulting in a natural synchronization with the electron beam. This solution allows us to directly measure the relative timing-jitter between the PC laser and the beam, as described in section 4.3. The encoding of the beam longitudinal profile is then obtained with the spatial decoding setup [31], in which the laser crosses the nonlinear crystal at an angle of 30°. Finally, the laser is imaged on a CCD camera as shown in figure 11(b). Each pixel corresponds to 10 fs.

5.2.1. Bunch duration measurements

The EOS station is located downstream the dogleg, 2 m far from the THz station. The EOS signals are obtained by using the 100 μm-thick GaP crystal, located 400 μm far from the traveling electron beam. Figure 12(a) shows a single-shot EOS signal acquired with the CCD camera after background subtraction. The temporal profile is calculated by projecting the acquired images along the vertical axis. The resulting signal is then fitted with a gaussian function, as shown in figure 12(b). The signal shows two negative valleys separated by a central positive peak. This behavior is due to a quarter-wave plate inserted between the EOS crystal and the exit polarizer, whose optical axis is slightly tilted with respect to the input laser polarization, ensuring a better sharpness of the output signal. It results that the laser cumulated a mean phase delay of $4.8° \pm 0.4°$, corresponding to a bunch peak electric field of about 3.3 MV m^{-1}. By averaging all the acquired shots, the resulting mean signal width is $\sigma_t = 95 \pm 5$ fs, in agreement with both GPT simulations (section 4.4) and CTR measurements (section 5.1.1).

5.2.2. Relative ATJ reduction downstream the dogleg

Being a single-shot device, the EOS can also be used as a time of arrival monitor measuring the relative ATJ between the electron beam and the probe laser. In figure 13 the time of arrival of 330 consecutive shots is reported. The rms of the resulting distribution is $\sigma_{t_{\mathrm{dogleg}}} = 19 \pm 5$ fs. Since the PC laser is used as the EOS reference, this value exactly represents the relative ATJ. This result confirms the validity of the model discussed in section 4.3, where we foresaw the reduction of the relative ATJ from 60 fs (downstream the linac) to 25 fs (downstream the dogleg). Although this value is slightly larger than the the experimental one, its discrepancy is limited to about 20%, confirming the validity of our assumptions.

6. Conclusions and future outlook

In this paper we discussed the longitudinal dynamics of a 50 pC beam compressed to approximately 90 fs (rms) by means of a hybrid compression scheme. It consists in the combined use of RF VB for the bunch shortening and and magnetic compression for the reduction of the ATJ relative to the PC laser. Measurements on the bunch duration, conducted both at the end of the linac and the dogleg, show that it is possible to take control of the longitudinal beam dynamics while reducing down to 19 fs (rms) the relative ATJ between the electron bunch and the external PC laser system. All the data (simulations and experimental measurements) are summarized in table 3. Results indicate that such ultra-short bunches, combined with fs-level laser-relative jitters, can be implemented in current seeded-FEL facilities. They could be also suitable for future laser-driven plasma accelerators that require the combined use of lasers and particle beams.

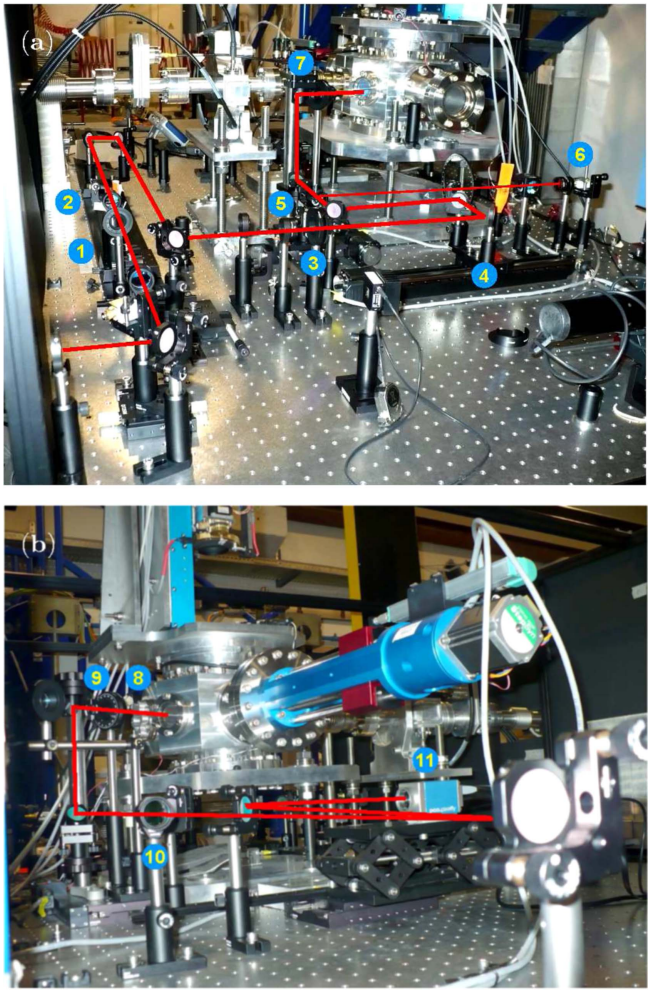

Figure 11. (a) Input layout. The laser crosses a telescopic system (1), beam splitter (2), half-wave plate (3) and an optical delay line (4), used for the fine synchronization between the laser and the electron beam. A beam splitter sends half laser to a photo-diode (6) and the other half to an horizontal polarizer (7). (b) Exit layout. A quarter-wave plate (8) is followed the second crossed polarizer (9), converting the polarization modulation in an intensity modulation. A lens (10) is used for the imaging of the crystal on the CCD (11).

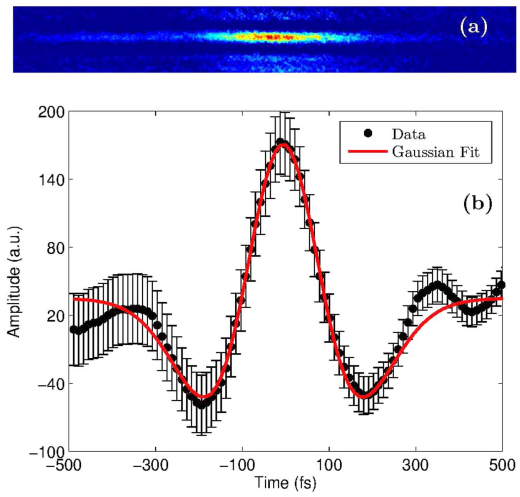

Figure 12. (a) EOS single-shot signal acquired by the CCD camera. (b) Temporal profile obtained by vertically projecting the EOS signal in (a). The signal width is $\sigma_t = 92 \pm 5$ fs.

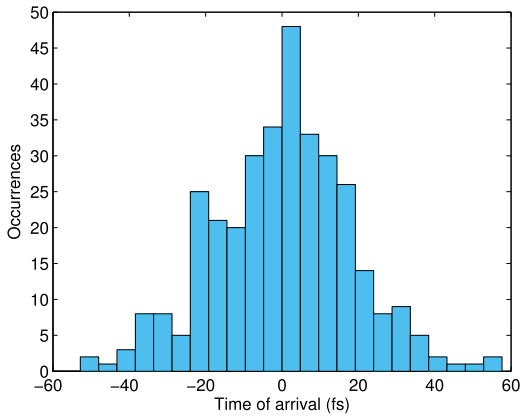

Figure 13. Collected time of arrival for 330 consecutive shots measured by the EOS. The resulting ATJ is $\sigma_t = 19 \pm 5$ fs.

Table 3. Summary of the achieved results.

Bunch duration	**Value (fs)**
Theoretical model (equation (4))	90
GPT simulation	92
Michelson interferometer	86 ± 7
Electro-optic sampling	95 ± 5
Relative ATJ	**Value (fs)**
Theoretical model (equation (18))	26
GPT simulation	25
Electro-optic sampling	19 ± 5

As a final remark, the hybrid compression can be further enhanced by using more flexible dogleg or magnetic chicane layouts. For instance, the R_{56} and T_{566} handling would be more effective by employing more than three quadrupoles and at least two sextupoles in the dispersive path. This would allow to achieve stronger bunch compressions with even lower relative timing-jitters.

Acknowledgments

This work has been partially supported by the EU Commission in the Seventh Framework Program, Grant Agreement 312453-EuCARD-2 and the Italian Research Minister in the framework of FIRB—Fondo per gli Investimenti della Ricerca di Base, project no. RBFR12NK5K.

References

[1] Giannessi L *et al* 2011 *Phys. Rev. Lett.* **106** 144801
[2] Chiadroni E *et al* 2013 *Rev. Sci. Instrum.* **84** 022703
[3] Litos M *et al* 2014 *Nature* **515** 92
[4] Luiten O, Van der Geer S, De Loos M, Kiewiet F and Van Der Wiel M 2004 *Phys. Rev. Lett.* **93** 094802
[5] Musumeci P, Moody J, England R, Rosenzweig J and Tran T 2008 *Phys. Rev. Lett.* **100** 244801
[6] Ferrario M *et al* 2013 *Nucl. Instrum. Methods Phys. Res. Sec.* B **309** 183
[7] Serafini L and Ferrario M 2001 *Am. Inst. Phys. Conf. Ser.* **581** 87–106
[8] Marchetti B, Bacci A, Chiadroni E, Cianchi A, Ferrario M, Mostacci A, Pompili R, Ronsivalle C, Spataro B and Zagorodnov I 2015 *Rev. Sci. Instrum.* **86** 073301
[9] Cavalieri A L *et al* 2005 *Phys. Rev. Lett.* **94** 114801
[10] Steffen B *et al* 2009 *Phys. Rev. ST Accel. Beams* **12** 032802
[11] Allaria E *et al* 2012 *New J. Phys.* **14** 113009
[12] Petralia A *et al* 2015 *Phys. Rev. Lett.* **115** 014801
[13] Bacci A *et al* 2013 *J. Appl. Phys.* **113** 194508
[14] Hidding B, Pretzler G, Rosenzweig J, Königstein T, Schiller D and Bruhwiler D 2012 *Phys. Rev. Lett.* **108** 035001
[15] Rossi A R *et al* 2014 *Nucl. Instrum. Methods Phys. Res.* A **740** 60
[16] Alesini D *et al* 2003 *Nucl. Instrum. Methods Phys. Res.* A **507** 345
[17] Gizzi L *et al* 2013 *Nucl. Instrum. Methods Phys. Res.* B **309** 202
[18] Levato T *et al* 2013 *Nucl. Instrum. Methods Phys. Res.* A **720** 95

[19] Petrillo V et al 2013 Phys. Rev. Lett. 111 114802
[20] Vaccarezza C et al 2016 Nucl. Instrum. Methods Phys. Res. A 829 237–42
[21] Chiadroni E et al 2013 Appl. Phys. Lett. 102 094101
[22] Giorgianni F et al 2016 Appl. Sci. 6 56
[23] Ferrario M et al 2011 Nucl. Instrum. Methods Phys. Res. A 637 43
[24] Villa F, Cialdi S, Anania M, Gatti G, Giorgianni F and Pompili R 2014 Nucl. Instrum. Methods Phys. Res. A 740 188
[25] Cianchi A et al 2008 Phys. Rev. ST Accel. Beams 11 032801
[26] Anderson S et al 2005 Phys. Rev. ST Accel. Beams 8 014401
[27] Pompili R et al 2016 Nucl. Instrum. Methods Phys. Res. A 829 17–23
[28] Ferrario M et al 2010 Phys. Rev. Lett. 104 054801
[29] Filippetto D et al 2011 Phys. Rev. ST Accel. Beams 14 092804
[30] Cianchi A 2015 Phys. Rev. ST Accel. Beams 18 082804
[31] Pompili R 2014 Nucl. Instrum. Methods Phys. Res. A 740 216
[32] Chiadroni E et al 2013 Rev. Sci. Instrum. 84 022703
[33] England R, Rosenzweig J, Andonian G, Musumeci P, Travish G and Yoder R 2005 Phys. Rev. ST Accel. Beams 8 012801
[34] Guetg M W, Beutner B, Prat E and Reiche S 2015 Phys. Rev. ST Accel. Beams 18 030701
[35] Sun Y et al 2011 Analysis on achieving a minimum bunch length in LCLS Bunch Compressor One Technical Report SLAC-PUB-14335 SLAC National Accelerator Laboratory
[36] Moody J, Musumeci P, Gutierrez M, Rosenzweig J and Scoby C 2009 Phys. Rev. ST Accel. Beams 12 070704
[37] De Loos M and Van der Geer S 1996 5th European Particle Accelerator Conf. p 1241
[38] Craievich P, Di Mitri S, Milloch M, Penco G and Rossi F 2013 Phys. Rev. ST Accel. Beams 16 090401
[39] Bellaveglia M et al 2015 Proc. SPIE 9512 95120V
[40] Alesini D, Di Pirro G, Ficcadenti L, Mostacci A, Palumbo L, Rosenzweig J and Vaccarezza C 2006 Nucl. Instrum. Methods Phys. Res. A 568 488
[41] Murokh A, Rosenzweig J, Hogan M, Suk H, Travish G and Happek U 1998 Nucl. Instrum. Methods Phys. Res. A 410 452
[42] Zhang Z et al 2014 Phys. Rev. ST Accel. Beams 17 032803
[43] Grote H and Schmidt F 2003 Proc. Particle Accelerator Conf. 2003 vol 5 (Piscataway, NJ: IEEE) pp 3497–9
[44] Giorgianni F et al 2015 Proc. SPIE 9509 95090O
[45] Castellano M, Cianchi A, Orlandi G and Verzilov V 1999 Nucl. Instrum. Methods Phys. Res. A 435 297
[46] Lai R, Happek U and Sievers A 1994 Phys. Rev. E 50 R4294
[47] Wilke I, MacLeod A M, Gillespie W, Berden G, Knippels G and Van Der Meer A 2002 Phys. Rev. Lett. 88 124801